Nanostructured Magnonic Crystals with Size-Tunable Bandgaps

Zhi Kui Wang,[†] Vanessa Li Zhang,[†] Hock Siah Lim,[†] Ser Choon Ng,[†] Meng Hau Kuok,[†,*] Shikha Jain,[‡] and Adekunle Olusola Adeyeye[‡,*]

[†]Department of Physics and [‡]Department of Electrical and Computer Engineering, National University of Singapore, Singapore 117542

ABSTRACT Just as a photonic crystal is a periodic composite composed of materials with different dielectric constants, its lesser known magnetic analogue, the magnonic crystal can be considered as a periodic composite comprising different magnetic materials. Magnonic crystals are excellent candidates for the fabrication of nanoscale microwave devices, as the wavelengths of magnons in magnonic crystals are orders of magnitude shorter than those of photons, of the same frequency, in photonic crystals. Using advanced electron beam lithographic techniques, we have fabricated a series of novel bicomponent magnonic crystals which exhibit well-defined frequency bandgaps. They are in the form of laterally patterned periodic arrays of alternating cobalt and permalloy stripes of various widths ranging from 150 to 500 nm. Investigations by Brillouin light scattering and computer modeling show that the dispersion spectrum of these crystals is strongly dependent on their structural dimensions. For instance, their first frequency bandgap is found to vary over a wide range of 1.4—2.6 gigahertz. Such a functionality permits the tailoring of the bandgap structure which controls the transmission of information-carrying spin waves in devices based on these crystals. Additionally, it is observed that the bandgap width decreases with increasing permalloy stripe width, but increases with increasing cobalt stripe width, and that the bandgap center frequency is more dependent on the stripe width of permalloy than that of cobalt. This information would be of value in the design of magnonic crystals for potential applications in the emerging field of magnonics.

KEYWORDS: magnonic crystals · magnonics · dispersion relations · frequency bandgaps · size tenability · Brillouin spectroscopy

While extensive research has been undertaken on photonic crystals,[1,2] information on their analogue, magnonic crystals is relatively scarce.[3−18] Frequency bandgaps, which are an intrinsic property of magnonic crystals, control how magnons (quantized spin waves) move through these crystals. Indeed, these crystals form the basis of magnonics, a nascent field which aims to control the generation and propagation of information-carrying magnons in a way analogous to the control of photons in photonic crystals. It is anticipated that magnonic crystals will have wide-ranging applications such as in magnetoelectronic devices[10] and magnonic waveguides.[11] Tunability of the frequency bandgap of magnonic crystals would be essential to the functioning of devices based on such crystals. We recently have investigated the magnetic-field tunability of a magnonic crystal in the form of a one-dimensional (1D) periodic array comprising nanostripes of alternating magnetic materials.[3]

Prior to our recent study of a bicomponent magnonic crystal,[3] bandgap experiments were confined to structures composed of only one constituent magnetic material.[16−22] The presence of a second magnetic material in our magnonic crystals provides another parameter with which to customize their band structure, for example the gap width and center frequency.

It has been predicted that, in general, the more contrasting the magnetic properties of the constituent materials of a magnonic crystal are, the wider would be its bandgap.[5,6] Because we wanted well-defined bandgaps, cobalt and permalloy ($Ni_{80}Fe_{20}$) were selected as fabrication materials, as the saturation magnetization and exchange constant of the former are about twice those of the latter. Ideally, magnonic crystals are to be engineered so that their bandgap can be tunable by, for example, changing their structural periodicity (lattice constant) or by the application of a magnetic field.[3] Bandgap tunability in devices based on these crystals will facilitate the control of the propagation of spin waves which act as information carriers.

Here we report on a study of the size tunability of a series of magnonic crystals in the form of laterally patterned periodic arrays of alternating contacting permalloy and cobalt nanostripes. Their magnon dispersions were mapped by Brillouin light scattering, a powerful nondestructive noncontact probe of spin waves in nanostructures.[22−27] Dependences of the

*Address correspondence to phykmh@nus.edu.sg, eleaao@nus.edu.sg.

Received for review September 7, 2009 and accepted January 15, 2010.

Published online January 25, 2010.
10.1021/nn901171u

© 2010 American Chemical Society

first magnonic bandgaps on the structural dimensions of the samples were measured as well as simulated by computer modeling.

RESULTS AND DISCUSSION

A novel method was employed for synthesizing the magnonic structures on an oxidized Si(001) substrate. Details of the fabrication process which is based on advanced lithographic techniques, briefly outlined in ref 3, are presented in this paper. A nanostripe array was first defined on a polymethyl methacrylate (PMMA) resist. This was followed by electron beam deposition and lift-off of a 30 nm-thick permalloy ($Ni_{80}Fe_{20}$) film, with the base pressure and deposition rate maintained at approximately 3×10^{-7} torr and 0.12 Å/s, respectively. The second nanostripe array was formed by first coating another layer of PMMA resist on the silicon substrate. The position of this array was defined using high-resolution electron beam lithography. A 30 nm-thick cobalt film was then deposited at a rate of 0.18 Å/s. Scanning electron microscope images of the resulting nanostructured array reveal that its alternating cobalt and permalloy stripes are very well-aligned.

A total of eleven crystals with periods (lattice constants) a = 300, 400, 500, 550, 600, 650, and 750 nm and stripe widths of 150, 250, 350, 400, and 500 nm were synthesized in this way. All stripes have a length of 100 μm and a thickness of 30 nm, and the length of each array is 100 μm. A crystal with respective cobalt and permalloy (Py) stripe widths of M and N nm will hereafter be referred to as MnmCo/NnmPy. In designing our crystals, their periodicities were chosen so that, for the experimentally accessible spin wave wavevectors, their dispersion spectra can be measured across at least a complete Brillouin zone (BZ). For instance, the dispersion spectrum of the 150nmCo/250nmPy sample is measurable up to its third BZ.

All Brillouin spectra were recorded in the 180°-backscattering geometry and in $p-s$ polarization using a six-pass tandem Fabry−Perot interferometer equipped with a silicon avalanche diode detector. The spectra were excited with 80 mW of the λ = 514.5 nm radiation of an argon-ion laser. Prior to the start of an experiment, each sample was saturated in a one-tesla field H directed parallel to the z-axis as shown in Figure 1a. Magnon dispersion relations (**H** = 0 T) can be mapped across Brillouin zones, that is, over magnon wavevector range q (= $4\pi \sin\theta/\lambda$) from 0 to $n\pi/a$ (n = integer), by varying the laser light incidence angle θ.

Figure 1 panels b and c show typical Brillouin spectra, those of the 150nmCo/250nmPy sample, recorded at various magnon wavevectors. Each spectrum contains up to three peaks due to spin wave modes, the frequencies of which were obtained from a fit with Lorentzian functions. The frequencies of the modes are plotted as a function of their wavevector in Figure 2a. It shows the three dispersion branches of the resulting

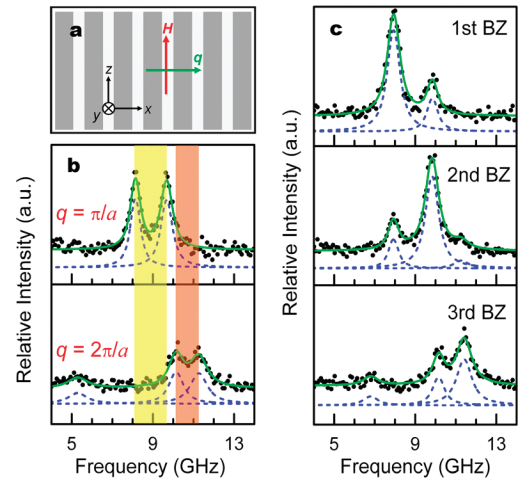

Figure 1. (a) Directions of applied magnetic field H for saturation of samples and magnon wavevector q relative to orientation of their nanostripes. (b) Brillouin spectra (H = 0) of 150nmCo/250nmPy crystal recorded at various Brillouin zone boundaries ($q = n\pi/a$). (c) Brillouin spectra (H = 0) recorded within various Brillouin zones. All spectra were fitted with Lorentzian functions (dashed curves), and the resultant fitted spectra are shown as solid curves.

periodic dispersion relations for spin waves in the sample, measured up to the third BZ. The magnonic dispersion spectrum features two direct frequency band-

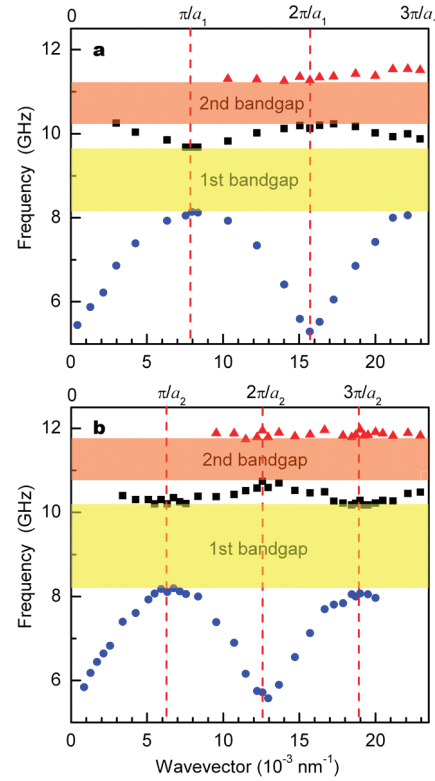

Figure 2. Measured dispersion relations, featuring bandgap structures, of spin waves in (a) 150nmCo/250nmPy, and (b) 250nmCo/250nmPy magnonic crystals, with respective lattice constants a_1 = 400 nm and a_2 = 500 nm. Experimental data are denoted by symbols. The first and second frequency bandgaps are represented by shaded bands, while the Brillouin zone boundaries ($q = n\pi/a$) are denoted by dashed lines.

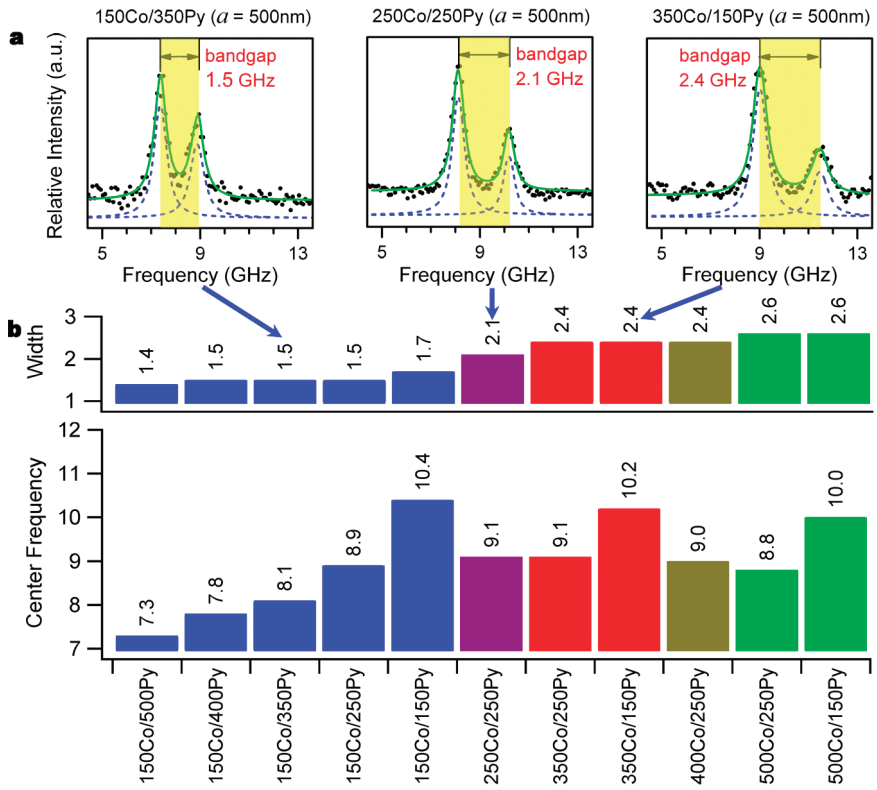

Figure 3. (a) Brillouin spectra of the 150nmCo/350nmPy, 250nmCo/250nmPy and 350nmCo/150nmPy samples recorded at the first Brillouin zone boundary $q = \pi/a$ (lattice constant $a = 500$ nm). (b) Measured values of the first bandgap widths and center frequencies, in GHz, of the 11 magnonic crystals studied.

gaps, with the first and second bandgap widths being 1.5 and 1.1 GHz, respectively. The dispersion spectra of the samples are modified by the sizes of their component stripes. For example, the dispersion relations for spin waves in the 250nmCo/250nmPy crystal, depicted in Figure 2b, show that its first and second bandgaps of 2.1 and 1.2 GHz are respectively wider than those of the 150nmCo/250nmPy one.

A notable spectral intensity pattern of the three Brillouin peaks was observed over the various BZs, as illustrated in Figure 1c for 150nmCo/250nmPy. The three spectra shown were each recorded for the same scanning duration. The maximal intensity of the lowest-energy peak lies within the first BZ, while those of the second and third lowest-energy peaks lie within the second and third BZs, respectively. This is theoretically expected as the Brillouin light scattering processes for peaks measured within their respective BZs are normal processes which do not involve the reciprocal lattice vector **G** ($G = n2\pi/a$, n is an integer).[28] In contrast, measurements of peaks made outside of their respective BZs (*e.g.*, the lowest-energy peak measured outside of the first BZ) entail the Umklapp process which involves **G**.[28] Hence, these peaks appear with lower intensity as this process involves an additional quasiparticle of momentum $\hbar\mathbf{G}$, where $2\pi\hbar$ = Planck constant. However, in the neighborhood of each Brillouin zone boundary, the intensities of the peaks arising from the same mode, within and outside their respective BZs, are about the same within experimental error.

Representative Brillouin spectra, those of samples with $a = 500$ nm, recorded at the first BZ boundary, are displayed in Figure 3a. They contain peaks, due to the two lowest-energy spin wave modes, the separation of which corresponds to the first bandgap width. The measured widths and center frequencies of the first bandgap of the eleven magnonic samples studied are presented in Figure 3b. It reveals that the values of the center frequencies lie between 7.3 GHz (150nmCo/500nmPy sample) and 10.4 GHz (150nmCo/150nmPy sample). It is noteworthy that the gap widths vary over a wide frequency range of 1.4−2.6 GHz, corresponding to the respective values for the 150nmCo/500nmPy and 500nmCo/250nmPy crystals.

Experimental data on the dependences of the first magnonic bandgap on the structural dimensions of all the samples investigated are summarized in Figure 4. It is noteworthy that the bandgap width decreases with increasing Py stripe width, but increases with increasing Co stripe width (Figure 4b,d). Specifically, for a fixed Py stripe width of 250 nm, as shown in Figure 4d, the gap width varies from 1.5 GHz (150 nm-wide Co stripe) to 2.6 GHz (500 nm-wide Co stripe), corresponding to a 73% increase. On the other hand for a constant Co stripe width of 150 nm, Figure 4b reveals that the gap width changes from 1.7 GHz (150 nm-wide Py stripe) to 1.4 GHz (500 nm-wide Py stripe), corresponding to a de-

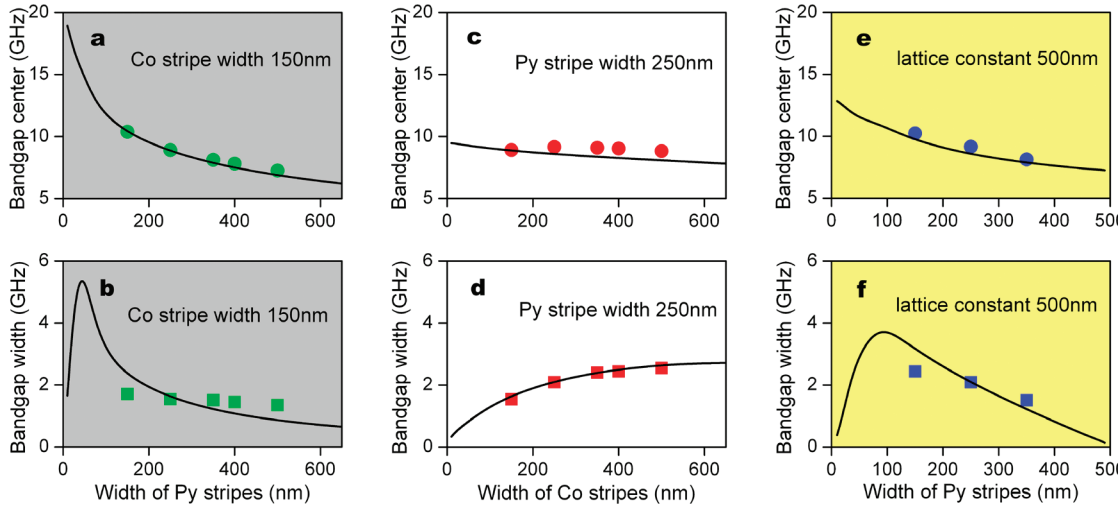

Figure 4. Dependences of first bandgap center frequencies and widths of magnonic crystals on (a, b) Py stripe width (Co stripe width = 150 nm), (c, d) Co stripe width (Py stripe width = 250 nm), and (e, f) Py stripe width (lattice constant = 500 nm). Experimental and theoretical data are represented by symbols and continuous lines, respectively.

crease of only 18%. In contrast with the gap width, from Figure 4 panels a and c, it is evident that the center frequency is more dependent on the stripe width of permalloy than that of cobalt. Figure 4 panels e and f illustrate how, for arrays with a common lattice constant of 500 nm, their bandgap parameters depend on the respective sizes of their component stripes. These interesting observations warrant further theoretical investigation.

Calculations of the first bandgap width and center frequency were carried out using the following approach. The magnetic stripes were treated as being infinitely long in the *z*-direction (see Figure 1a). For zero applied magnetic field, linearization of the Landau−Lifshitz equation yields[29]

$$i\Omega m_x(\mathbf{r}) + (\nabla\cdot Q\nabla)m_y(\mathbf{r}) - M_s\frac{\partial\Psi(\mathbf{r})}{\partial y} = 0 \qquad (1)$$

and

$$i\Omega m_y(\mathbf{r}) - (\nabla\cdot Q\nabla)m_x(\mathbf{r}) + M_s\frac{\partial\Psi(\mathbf{r})}{\partial x} = 0 \qquad (2)$$

where $\Omega = \omega/(\mu_0\gamma)$, $Q = 2A/(\mu_0 M_s)$, A is the exchange constant, M_s the saturation magnetization, γ the gyromagnetic ratio, m_x and m_y the components of the dynamical magnetization **m**, and ω the spin wave angular frequency. Outside the stripes, the magnetic potential $\Psi(\mathbf{r})$ satisfies the Laplace equation, while inside, the following equation holds

$$\nabla^2\Psi(\mathbf{r}) = \frac{\partial m_x(\mathbf{r})}{\partial x} + \frac{\partial m_y(\mathbf{r})}{\partial y} \qquad (3)$$

The usual magnetostatic boundary conditions were imposed. For simplicity, surface/interface energy anisotropy was neglected. Hence, at the interfaces between cobalt and permalloy stripes, the exchange boundary conditions require the continuity of the magnetization **m** and $(A/M_s)(\partial\mathbf{m}/\partial x)$.[30] As the propagating spin waves are modulated by the periodicity of the magnonic crystal, the Bloch theorem yields $\mathbf{m}(x + a, y) = \mathbf{m}(x,y)\exp(iqa)$ and $\Psi(x + a, y) = \Psi(x,y)\exp(iqa)$, where a is the lattice constant of the crystal. Solving eqs 1−3 numerically for $q = \pi/a$ (BZ boundary) allows the evaluation of the bandgap width and center frequency. The evaluation was based on the magnetic parameters $M_s = 1.15 \times 10^6$ A/m, $A = 2.88 \times 10^{-11}$ J/m, $\gamma = 198.8$ GHz/T for cobalt, and $M_s = 6.58 \times 10^5$ A/m, $A = 1.11 \times 10^{-11}$ J/m, $\gamma = 190.5$ GHz/T for permalloy. These parameters were obtained from least-squares fits to data derived from Brillouin spectroscopic measurements of 30 nm-thick cobalt and permalloy reference films. It should be pointed out that only the magnetic parameters of the reference cobalt and permalloy films were used in the calculations. The computed dependences are presented in the Figure 4. Despite the simplicity of the model employed, there is good general agreement between calculations and measurements. The quantitative discrepancy could be a consequence of neglecting the cobalt−permalloy interface exchange interaction and surface/interface energy anisotropy in our model. However detailed information on them are currently not available. Hence, the degree of surface/interface pinning and the effect of interface exchange coupling require further investigation. Our Brillouin experiments probed spin waves propagating along the one-dimensional magnonic crystals, and not spin waves localized in any component nanostripe. The measured magnon wavevectors q range from 0.04×10^7 to 2.3×10^7 m^{-1}, and whether the long-range dipole−dipole interactions or the short-range exchange effects predominate depends on q. In general, dipole−dipole interactions dominate over the exchange effects for $q < 10^7$ m^{-1}, while exchange effects are dominant for $q > 10^8$ m^{-1}, and within the intermediate regime, the two interactions are comparable.[31]

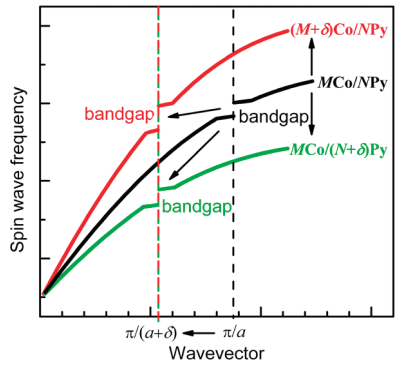

Figure 5. Schematic dispersion relation to illustrate the dependence of bandgap center frequency on the respective cobalt and permalloy stripe widths.

A simple qualitative explanation of the observed dependence of the bandgap center parameters on the respective widths of the Co and Py stripes is now presented. The black curve of the schematic diagram (Figure 5) represents the dispersion of a reference *M*nmCo/*N*nmPy sample. Since the saturation magnetization M_s and exchange constant *A* of Co are about twice those of Py, an increase in the Co stripe width by δ nm, with Py stripe width fixed, will increase the mean values of M_s and *A* of the $(M + \delta)$nmCo/*N*nmPy sample, resulting in an increase in magnon frequencies (red dispersion curve) relative to the reference sample (black dispersion curve). On the other hand, an increase in the Py stripe width by δ nm, with Co stripe width fixed, will decrease the mean values of M_s and *A* of the *M*nmCo/$(N + \delta)$nmPy sample resulting in a decrease in magnon frequencies (green dispersion curve). It is to be noted that an increase in either the Co or Py stripe width would cause a reduction of the first BZ boundary from π/a to $\pi/(a + \delta)$, where the lattice constant $a = M + N$. The change in the bandgap center frequency with change in stripe width depends on these two factors. In the case of increasing Py stripe width, the two factors reinforce each other, resulting in a larger change in center frequency, as shown in Figure 4a. However, in the case of increasing the Co stripe width, the two factors oppose each other, resulting in a smaller change, in agreement with Figure 4c. Hence, the center frequency is more dependent on the Py stripe width than that of Co.

In general, the bandgap width will depend on the relative magnetic contrasts of the constituent materials,[5,6] namely M_s(Co)/M_s(Py) and *A*(Co)/*A*(Py), both of which are of the order of two. Consider the reference magnonic crystal to be one where $M = N = d$, say. In this case, its gap width $\sim M_s(\text{Co})/M_s(\text{Py}) = [dM_s(\text{Co})]/[dM_s(\text{Py})]$. To see how the gap width varies with the Co stripe width, we make a Taylor's expansion, yielding a gap width $\sim (1 + \delta/d)M_s(\text{Co})/M_s(\text{Py})$, where δ is a small increase in the Co stripe width. This shows the gap width increases with increasing Co stripe width, in agreement with measurements (see Figure 4d). On the other hand, a widening of the Py stripe by δ, would result in a gap width $\sim (1 - \delta/d)M_s(\text{Co})/M_s(\text{Py})$, that is, the gap width decreases with increasing Py stripe width, as depicted in Figure 4b. Similar arguments can be applied to the exchange constant contrast *A*(Co)/*A*(Py) to account for the observation that the bandgap width decreases with increasing Py stripe width, but increases with increasing Co stripe width.

CONCLUSIONS

We have experimentally and theoretically investigated the spin dynamics of novel bicomponent nanostructured magnonic crystals which exhibit well-defined frequency bandgaps. By individually varying the widths of their permalloy and cobalt stripes, the magnonic dispersion spectrum of the crystals studied can be drastically modified. For instance, their first bandgap could be varied over a wide frequency range of 1.4−2.6 GHz. Such a functionality permits the tailoring of the bandgap structure which controls the transmission of information-carrying spin waves in devises based on these crystals. Interestingly, the bandgap width and center frequency exhibit contrasting dependences on the respective permalloy and cobalt stripe widths. Although our model did not take into account the surface/interface energy anisotropy and interface exchange coupling, theory accords fairly well with experimental Brillouin data. Our findings on the dispersion spectrum and the dependence of the bandgap structure on crystal dimensions should contribute to the further development of the theory and applications of magnonics, a nascent field which holds great promise in technologies such as microwave communications. Additionally, as the wavelengths of magnons in magnonic crystals are orders of magnitude shorter than those of photons, of the same frequency, in photonic crystals, magnonic crystals are excellent candidates for the fabrication of nanoscale microwave devices.

METHODS

Fabrication of Magnonic Crystals. The structures were fabricated using high-resolution multilevel electron beam lithography (EBL), deposition, and lift-off processes. A 120 nm-thick polymethyl methacrylate (PMMA) EBL resist was first spin-coated on an oxidized Si (001) wafer substrate. The substrate was baked at 180 °C for 90 s on a hot plate. The patterning of the first layer of stripes was performed using a 75 kV lithography system (Elionix ELS 7700) with a resist dose of 768 μC/cm^2. Appropriate alignment marks needed for the second stage of lithography process were also patterned at this stage. After the exposure, the substrate was developed in a 1:3 solution of methyl isobutyle ketone (MIBK) and isopropyl alcohol (IPA). A 30 nm-thick $Ni_{80}Fe_{20}$ film was then deposited at a rate of 0.12 Å/s on the patterned substrate in an electron beam deposition chamber with a base pressure of 3×10^{-7} torr. After the lift-off process in acetone, the

fabricated $Ni_{80}Fe_{20}$ stripes were examined under a JEOL JSM-6700F field emission SEM. The alignment marks fabricated in the first EBL stage were used in exposing the second set of stripes in the gaps between neighboring $Ni_{80}Fe_{20}$ stripes. The fabrication process was then repeated for the deposition of 30 nm-thick cobalt stripes at a rate of 0.18 Å/s, followed by a lift-off process. The final samples were imaged in SEM, revealing that they are one-dimensional magnonic crystals composed of alternating $Ni_{80}Fe_{20}$ and cobalt stripes of various widths.

Brillouin Light Scattering. Brillouin spectra were measured using a JRS Scientific Instruments (3 + 3)-pass tandem Fabry−Perot interferometer, of finesse about 120, equipped with a PerkinElmer SPCM-AQR-16 single photon-counting (silicon avalanche diode) module. The free spectral range of the interferometer was typically set at 20 GHz. The 514.5 nm radiation of a Spectra Physics 2080−15S argon-ion laser, operating in single mode, was used to excited the spectra, with a typical beam power of 80 mW incident on the samples. A continuous stream of pure argon gas was directed at the irradiated spot on the sample surface to cool it and to keep air away from it. All experiments were performed in the 180°-backscattering geometry and in $p-s$ polarization, with the scattered light passing through a Glan−Thompson polarizing prism. By varying the incidence angle of the laser light, the magnon dispersion relations were mapped across several Brillouin zones.

Acknowledgment. This study was funded by the Ministry of Education Singapore, under research projects R144-000-239-112 and R144-000-205-112.

REFERENCES AND NOTES

1. Vlasov, Y. A.; Bo, X. Z.; Sturm, J. C.; Norris, D. J. On-Chip Natural Assembly of Silicon Photonic Bandgap Crystals. *Nature (London)* **2001**, *414*, 289–293.
2. Joannopoulos, J. D.; Villeneuve, P. R.; Fan, S. Photonic Crystals: Putting a New Twist on Light. *Nature* **1997**, *386*, 143–149.
3. Wang, Z. K.; Zhang, V. L.; Lim, H. S.; Ng, S. C.; Kuok, M. H.; Jain, S.; Adeyeye, A. O. Observation of Frequency Band Gaps in a One-Dimensional Nanostructured Magnonic Crystal. *Appl. Phys. Lett.* **2009**, *94*, 083112.
4. Lee, K. S.; Han, D. S.; Kim, S. K. Physical Origin and Generic Control of Magnonic Band Gaps of Dipole-Exchange Spin Waves in Width-Modulated Nanostrip Waveguides. *Phys. Rev. Lett.* **2009**, *102*, 127202.
5. Krawczyk, M.; Puszkarski, H. Plane-Wave Theory of Three-Dimensional Magnonic Crystals. *Phys. Rev. B* **2008**, *77*, 054437.
6. Puszkarski, H.; Krawczyk, M. Magnonic Crystals—The Magnetic Counterpart of Photonic Crystals. *Solid State Phenom.* **2003**, *94*, 125–134.
7. Kruglyak, V. V.; Hicken, R. J. Magnonics: Experiment to Prove the Concept. *J. Magn. Magn. Mater.* **2006**, *306*, 191–194.
8. Nikitov, S. A.; Tsai, C. S.; Gulyaev, Y. V.; Filimonov, Y. A.; Volkov, A. I.; Vysotskii, S. L.; Tailhades, P. YIG Thin Film-Based Two-Dimensional Magnonic and Magneto-photonic Crystals. *Mater. Res. Soc. Symp. Proc.* **2005**, *834*, 87–96.
9. Nikitov, S. A.; Tailhades, P.; Tsai, C. S. Spin Waves in Periodic Magnetic Structures—Magnonic Crystals. *J. Magn. Magn. Mater.* **2001**, *236*, 320–330.
10. Kruglyak, V. V.; Kuchko, A. N. Spectrum of Spin Waves Propagating in a Periodic Magnetic Structure. *Phys. B* **2003**, *339*, 130–133.
11. Xi, H.; Wang, X.; Zheng, Y.; Ryan, P. J. Spinwave Propagation in Lossless Cylindrical Magnonic Waveguides. *J. Appl. Phys.* **2009**, *105*, 07A502.
12. Neusser, S.; Grundler, D. Magnonics: Spin Waves on the Nanoscale. *Adv. Mater.* **2009**, *21*, 2927–2932.
13. Krawczyk, M.; Puszkarski, H. Magnonic Crystal Theory of the Spin-Wave Frequency Gap in Low-Doped Manganites. *J. Appl. Phys.* **2006**, *100*, 073905.
14. Lee, K. S.; Kim, S. K. Conceptual Design of Spin Wave Logic Gates Based on a Mach−Zehnder-Type Spin Wave Interferometer for Universal Logic Functions. *J. Appl. Phys.* **2009**, *104*, 053909.
15. Kozhanov, A.; Ouellette, D.; Griffith, Z.; Rodwell, M.; Jacob, A. P.; Lee, D. W.; Wang, S. X.; Allen, S. J. Dispersion in Magnetostatic CoTaZr Spin Waveguides. *Appl. Phys. Lett.* **2009**, *94*, 012505.
16. Chumak, A. V.; Serga, A. A.; Wolff, S.; Hillebrands, B.; Kostylev, M. P. Design and Optimization of One-Dimensional Ferrite-Film Based Magnonic Crystals. *J. Appl. Phys.* **2009**, *105*, 083906.
17. Chumak, A. V.; Serga, A. A.; Wolff, S.; Hillebrands, B.; Kostylev, M. P. Scattering of Surface and Volume Spin Waves in a Magnonic Crystal. *Appl. Phys. Lett.* **2009**, *94*, 172511.
18. Chumak, A. V.; Serga, A. A.; Hillebrands, B.; Kostylev, M. P. Scattering of Backward Spin Waves in a One-Dimensional Magnonic Crystal. *Appl. Phys. Lett.* **2008**, *93*, 022508.
19. Gulyaev, Y. V.; Nikitov, S. A.; Zhivotovskii, L. V.; Klimov, A. A.; Tailhades, P.; Presmanes, L.; Bonningue, C.; Tsai, C. S.; Vysotskii, S. L.; Filimonov, Y. A. Ferromagnetic Films with Magnon Bandgap Periodic Structures: Magnon Crystals. *J. Exp. Theor. Phys.* **2003**, *77*, 567–570.
20. Vysotskii, S. L.; Nikitov, S. A.; Filimonov, Y. A. Magnetostatic Spin Waves in Two-Dimensional Periodic Structures (Magnetophoton Crystals). *J. Exp. Theor. Phys.* **2005**, *101*, 547–553.
21. Dokukin, M. E.; Togo, K.; Inoue, M. Propagation of Magnetostatic Surface Waves in a Tunable One-Dimensional Magnonic Crystal. *J. Magn. Soc. Jpn.* **2008**, *32*, 103–105.
22. Kostylev, M.; Schrader, P.; Stamps, R. L.; Gubbiotti, G.; Carlotti, G.; Adeyeye, A. O.; Goolaup, S.; Singh, N. Partial Frequency Band Gap in One-Dimensional Magnonic Crystals. *Appl. Phys. Lett.* **2008**, *92*, 132504.
23. Wang, Z. K.; Kuok, M. H.; Ng, S. C.; Lockwood, D. J.; Cottam, M. G.; Nielsch, K.; Wehrspohn, R. B.; Gosele, U. Spin-Wave Quantization in Ferromagnetic Nickel Nanowires. *Phys. Rev. Lett.* **2002**, *89*, 027201.
24. Wang, Z. K.; Lim, H. S.; Zhang, V. L.; Goh, J. L.; Ng, S. C.; Kuok, M. H.; Su, H. L.; Tang, S. L. Collective Spin Waves in High-Density Two-Dimensional Arrays of FeCo Nanowires. *Nano Lett.* **2006**, *6*, 1083–1086.
25. Wang, Z. K.; Lim, H. S.; Liu, H. Y.; Ng, S. C.; Kuok, M. H.; Tay, L. L.; Lockwood, D. J.; Cottam, M. G.; Hobbs, K. L.; Larson, P. R.; *et al.* Spin Waves in Nickel Nanorings of Large Aspect Ratio. *Phys. Rev. Lett.* **2005**, *94*, 137208.
26. Demokritov, S. O.; Hillebrands, B.; Slavin, A. N. Brillouin Light Scattering Studies of Confined Spin Waves: Linear And Nonlinear Confinement. *Phys. Rep.* **2001**, *348*, 441–489.
27. Mathieu, C.; Jorzick, J.; Frank, A.; Demokritov, S. O.; Slavin, A. N.; Hillebrands, B.; Bartenlian, B.; Chappert, C.; Decanini, D.; Rousseaux, F.; Cambril, E. Lateral Quantization of Spin Waves in Micron Size Magnetic Wires. *Phys. Rev. Lett.* **1998**, *81*, 3968–3971.
28. Kittel, C. *Introduction to Solid State Physics*, 8th ed.; John Wiley & Sons, Inc: New York, 2005.
29. Vasseur, J. O.; Dobrzynski, L.; Djafari-Rouhani, B.; Puszkarski, H. Magnon Band Structure of Periodic Composites. *Phys. Rev. B* **1996**, *54*, 1043–1049.
30. Kruglyak, V. V.; Hicken, R. J.; Kuchko, A. N.; Gorobets, V. Y. Spin Waves in a Periodically Layered Magnetic Nanowire. *J. Appl. Phys.* **2005**, *98*, 014304.
31. Cottam, M. G. Lockwood D. J. *Light Scattering in Magnetic Solids*; John Wiley & Sons, Inc: New York, 1986.